Ultra low noise Fourier domain mode locked laser for high quality megahertz optical coherence tomography

TOM PFEIFFER,[1,2] MARKUS PETERMANN,[3] WOLFGANG DRAXINGER,[1,2] CHRISTIAN JIRAUSCHEK,[4] AND ROBERT HUBER[1,2,*]

[1]*Institut für Biomedizinische Optik, Universität zu Lübeck, Peter-Monnik-Weg 4, 23562 Lübeck, Germany*
[2]*Medizinisches Laserzentrum Lübeck GmbH, Peter-Monnik-Weg 4, 23562 Lübeck, Germany*
[3]*Optores GmbH, Gollierstr. 70, 80339 Munich, Germany*
[4]*Department of Electrical and Computer Engineering, Technical University of Munich (TUM), Arcisstraße 21, 80333 Munich, Germany*
*Robert.Huber@bmo.uni-luebeck.de

Abstract: We investigate the origin of high frequency noise in Fourier domain mode locked (FDML) lasers and present an extremely well dispersion compensated setup which virtually eliminates intensity noise and dramatically improves coherence properties. We show optical coherence tomography (OCT) imaging at 3.2 MHz A-scan rate and demonstrate the positive impact of the described improvements on the image quality. Especially in highly scattering samples, at specular reflections and for strong signals at large depth, the noise in optical coherence tomography images is significantly reduced. We also describe a simple model that suggests a passive physical stabilizing mechanism that leads to an automatic compensation of remaining cavity dispersion in FDML lasers.

References and links

1. R. Huber, M. Wojtkowski, and J. G. Fujimoto, "Fourier Domain Mode Locking (FDML): A new laser operating regime and applications for optical coherence tomography," Opt. Express **14**(8), 3225–3237 (2006).
2. D. Huang, E. A. Swanson, C. P. Lin, J. S. Schuman, W. G. Stinson, W. Chang, M. R. Hee, T. Flotte, K. Gregory, C. A. Puliafito, and J. G. Fujimoto, "Optical coherence tomography," Science **254**(5035), 1178–1181 (1991).
3. W. Wieser, B. R. Biedermann, T. Klein, C. M. Eigenwillig, and R. Huber, "Multi-megahertz OCT: High quality 3D imaging at 20 million A-scans and 4.5 GVoxels per second," Opt. Express **18**(14), 14685–14704 (2010).
4. B. R. Biedermann, W. Wieser, C. M. Eigenwillig, G. Palte, D. C. Adler, V. J. Srinivasan, J. G. Fujimoto, and R. Huber, "Real time en face Fourier-domain optical coherence tomography with direct hardware frequency demodulation," Opt. Lett. **33**(21), 2556–2558 (2008).
5. D. C. Adler, W. Wieser, F. Trepanier, J. M. Schmitt, and R. A. Huber, "Extended coherence length Fourier domain mode locked lasers at 1310 nm," Opt. Express **19**(21), 20930–20939 (2011).
6. L. Reznicek, T. Klein, W. Wieser, M. Kernt, A. Wolf, C. Haritoglou, A. Kampik, R. Huber, and A. S. Neubauer, "Megahertz ultra-wide-field swept-source retina optical coherence tomography compared to current existing imaging devices," Graefes Arch. Clin. Exp. Ophthalmol. **252**(6), 1009–1016 (2014).
7. T. Klein, R. André, W. Wieser, T. Pfeiffer, and R. Huber, "Joint aperture detection for speckle reduction and increased collection efficiency in ophthalmic MHz OCT," Biomed. Opt. Express **4**(4), 619–634 (2013).
8. B. R. Biedermann, W. Wieser, C. M. Eigenwillig, and R. Huber, "Recent developments in Fourier Domain Mode Locked lasers for optical coherence tomography: Imaging at 1310 nm vs. 1550 nm wavelength," J. Biophotonics **2**(6-7), 357–363 (2009).
9. S. Karpf, M. Eibl, W. Wieser, T. Klein, and R. Huber, "A Time-Encoded Technique for fibre-based hyperspectral broadband stimulated Raman microscopy," Nat. Commun. **6**(1), 6784 (2015).
10. C. M. Eigenwillig, W. Wieser, S. Todor, B. R. Biedermann, T. Klein, C. Jirauschek, and R. Huber, "Picosecond pulses from wavelength-swept continuous-wave Fourier domain mode-locked lasers," Nat. Commun. **4**(1), 1848 (2013).
11. L. A. Kranendonk, X. An, A. W. Caswell, R. E. Herold, S. T. Sanders, R. Huber, J. G. Fujimoto, Y. Okura, and Y. Urata, "High speed engine gas thermometry by Fourier-domain mode-locked laser absorption spectroscopy," Opt. Express **15**(23), 15115–15128 (2007).

12. D. Chen, C. Shu, and S. He, "Multiple fiber Bragg grating interrogation based on a spectrum-limited Fourier domain mode-locking fiber laser," Opt. Lett. **33**(13), 1395–1397 (2008).

13. E. J. Jung, C.-S. Kim, M. Y. Jeong, M. K. Kim, M. Y. Jeon, W. Jung, and Z. Chen, "Characterization of FBG sensor interrogation based on a FDML wavelength swept laser," Opt. Express **16**(21), 16552–16560 (2008).

14. B. C. Lee and M. Y. Jeon, "Remote fiber sensor based on cascaded Fourier domain mode-locked laser," Opt. Commun. **284**(19), 4607–4610 (2011).

15. L. Byoung Chang, J. Eun-Joo, K. Chang-Seok, and J. Min Yong, "Dynamic and static strain fiber Bragg grating sensor interrogation with a 1.3 μm Fourier domain mode-locked wavelength-swept laser," Meas. Sci. Technol. **21**(9), 094008 (2010).

16. J. Mei, X. Xiao, and C. Yang, "Delay Compensated FBG Demodulation System Based on Fourier Domain Mode-Locked Lasers," IEEE Photonics Technol. Lett. **27**(15), 1585–1588 (2015).

17. Y. Wang, W. Liu, J. Fu, and D. Chen, "Quasi-distributed fiber Bragg grating sensor system based on a Fourier domain mode locking fiber laser," Laser Phys. **19**(3), 450–454 (2009).

18. L. A. Kranendonk, R. Huber, J. G. Fujimoto, and S. T. Sanders, "Wavelength-agile H2O absorption spectrometer for thermometry of general combustion gases," Proc. Combust. Inst. **31**(1), 783–790 (2007).

19. J. P. Kolb, T. Klein, C. L. Kufner, W. Wieser, A. S. Neubauer, and R. Huber, "Ultra-widefield retinal MHz-OCT imaging with up to 100 degrees viewing angle," Biomed. Opt. Express **6**(5), 1534–1552 (2015).

20. J. P. Kolb, T. Klein, K. J. Mohler, W. Wieser, L. Reznicek, M. Kernt, A. Kampik, A. S. Neubauer, and R. Huber, "Choroidal, retinal and RPE thickness in diabetic retinopathy measured with widefield MHz-OCT over 60° field of view," Invest. Ophthalmol. Vis. Sci. **56**, 603 (2015).

21. W. Wieser, W. Draxinger, T. Klein, S. Karpf, T. Pfeiffer, and R. Huber, "High definition live 3D-OCT in vivo: design and evaluation of a 4D OCT engine with 1 GVoxel/s," Biomed. Opt. Express **5**(9), 2963–2977 (2014).

22. T. Wang, T. Pfeiffer, E. Regar, W. Wieser, H. van Beusekom, C. T. Lancee, G. Springeling, I. Krabbendam, A. F. W. van der Steen, R. Huber, and G. van Soest, "Heartbeat OCT: in vivo intravascular megahertz-optical coherence tomography," Biomed. Opt. Express **6**(12), 5021–5032 (2015).

23. T. Wang, W. Wieser, G. Springeling, R. Beurskens, C. T. Lancee, T. Pfeiffer, A. F. W. van der Steen, R. Huber, and G. van Soest, "Intravascular optical coherence tomography imaging at 3200 frames per second," Opt. Lett. **38**(10), 1715–1717 (2013).

24. C. Jirauschek, B. Biedermann, and R. Huber, "A theoretical description of Fourier domain mode locked lasers," Opt. Express **17**(26), 24013–24019 (2009).

25. C. Jirauschek and R. Huber, "Wavelength shifting of intra-cavity photons: Adiabatic wavelength tuning in rapidly wavelength-swept lasers," Biomed. Opt. Express **6**(7), 2448–2465 (2015).

26. C. Jirauschek and R. Huber, "Modeling and analysis of polarization effects in Fourier domain mode-locked lasers," Opt. Lett. **40**(10), 2385–2388 (2015).

27. S. Slepneva, B. Kelleher, B. O'Shaughnessy, S. P. Hegarty, A. G. Vladimirov, and G. Huyet, "Dynamics of Fourier domain mode-locked lasers," Opt. Express **21**(16), 19240–19251 (2013).

28. S. Todor, B. Biedermann, W. Wieser, R. Huber, and C. Jirauschek, "Instantaneous lineshape analysis of Fourier domain mode-locked lasers," Opt. Express **19**(9), 8802–8807 (2011).

29. C. Jirauschek and R. Huber, "Efficient simulation of the swept-waveform polarization dynamics in fiber spools and Fourier domain mode-locked (FDML) lasers," J. Opt. Soc. Am. B **34**(6), 1135–1146 (2017).

30. B. R. Biedermann, W. Wieser, C. M. Eigenwillig, T. Klein, and R. Huber, "Dispersion, coherence and noise of Fourier domain mode locked lasers," Opt. Express **17**(12), 9947–9961 (2009).

31. D. C. Adler, W. Wieser, F. Trepanier, J. M. Schmitt, and R. A. Huber, "Extended coherence length Fourier domain mode locked lasers at 1310 nm," Opt. Express **19**(21), 20930–20939 (2011).

32. W. Wieser, T. Klein, D. C. Adler, F. Trépanier, C. M. Eigenwillig, S. Karpf, J. M. Schmitt, and R. Huber, "Extended coherence length megahertz FDML and its application for anterior segment imaging," Biomed. Opt. Express **3**(10), 2647–2657 (2012).

33. T. Kraetschmer and S. T. Sanders, "Ultrastable Fourier Domain Mode Locking Observed in a Laser Sweeping 1363.8 - 1367.3 nm," in *Conference on Lasers and Electro-Optics/International Quantum Electronics Conference*, OSA Technical Digest (CD) (Optical Society of America, 2009), CFB4.

34. R. Huber, D. C. Adler, and J. G. Fujimoto, "Buffered Fourier domain mode locking: Unidirectional swept laser sources for optical coherence tomography imaging at 370,000 lines/s," Opt. Lett. **31**(20), 2975–2977 (2006).

35. R. Huber, M. Wojtkowski, K. Taira, J. Fujimoto, and K. Hsu, "Amplified, frequency swept lasers for frequency domain reflectometry and OCT imaging: design and scaling principles," Opt. Express **13**(9), 3513–3528 (2005).

36. R. Huber, M. Wojtkowski, J. G. Fujimoto, J. Y. Jiang, and A. E. Cable, "Three-dimensional and C-mode OCT imaging with a compact, frequency swept laser source at 1300 nm," Opt. Express **13**(26), 10523–10538 (2005).

37. T. Pfeiffer and R. Huber, "Verfahren zur Erhaltung der Synchronität eines Fourier Domain Mode Locked (FDML) Lasers," DE 10 2017 209 739.6 (2018).

38. T. Pfeiffer, W. Draxinger, W. Wieser, T. Klein, M. Petermann, and R. Huber, "Analysis of FDML lasers with meter range coherence," Proc. SPIE **10053**, 100531T (2017).

39. S. Slepneva, B. O'Shaughnessy, S. Hegarty, B. Kelleher, S. Rica, and G. Huyet, "Convective Nozaki-Bekki holes in a long cavity laser," Proc. SPIE **9732**, 97320F (2016).

40. H. Chaté and P. Manneville, "Stability of the Bekki-Nozaki hole solutions to the one-dimensional complex Ginzburg-Landau equation," Phys. Lett. A **171**(3-4), 183–188 (1992).

41. N. Bekki and K. Nozaki, "Formations of spatial patterns and holes in the generalized Ginzburg-Landau equation," Phys. Lett. A **110**(3), 133–135 (1985).
42. W. Wieser, G. Palte, C. M. Eigenwillig, B. R. Biedermann, T. Pfeiffer, and R. Huber, "Chromatic polarization effects of swept waveforms in FDML lasers and fiber spools," Opt. Express **20**(9), 9819–9832 (2012).
43. S. Slepneva, B. O'Shaughnessy, A. Vladimirov, S. Rica, and G. Huyet, "Turbulent laser puffs," arXiv:1801.05509 (2018).
44. M. Szkulmowski and M. Wojtkowski, "Averaging techniques for OCT imaging," Opt. Express **21**(8), 9757–9773 (2013).
45. H. T. Peter and K. W. Ruikang, "Digital phase stabilization to improve detection sensitivity for optical coherence tomography," Meas. Sci. Technol. **18**(11), 3365–3372 (2007).
46. N. D. Shemonski, F. A. South, Y.-Z. Liu, S. G. Adie, P. S. Carney, and S. A. Boppart, "Computational high-resolution optical imaging of the living human retina," Nat. Photonics **9**(7), 440–443 (2015).
47. W. Y. Oh, S. H. Yun, B. J. Vakoc, M. Shishkov, A. E. Desjardins, B. H. Park, J. F. de Boer, G. J. Tearney, and B. E. Bouma, "High-speed polarization sensitive optical frequency domain imaging with frequency multiplexing," Opt. Express **16**(2), 1096–1103 (2008).
48. M. Yamanari, S. Makita, and Y. Yasuno, "Polarization-sensitive swept-source optical coherence tomography with continuous source polarization modulation," Opt. Express **16**(8), 5892–5906 (2008).
49. M. Bonesi, H. Sattmann, T. Torzicky, S. Zotter, B. Baumann, M. Pircher, E. Götzinger, C. Eigenwillig, W. Wieser, R. Huber, and C. K. Hitzenberger, "High-speed polarization sensitive optical coherence tomography scan engine based on Fourier domain mode locked laser," Biomed. Opt. Express **3**(11), 2987–3000 (2012).
50. S. Makita, Y. Hong, M. Yamanari, T. Yatagai, and Y. Yasuno, "Optical coherence angiography," Opt. Express **14**(17), 7821–7840 (2006).
51. B. Vakoc, S. Yun, J. de Boer, G. Tearney, and B. Bouma, "Phase-resolved optical frequency domain imaging," Opt. Express **13**(14), 5483–5493 (2005).
52. M. Eibl, S. Karpf, W. Wieser, T. Klein, and R. Huber, "Hyperspectral stimulated Raman microscopy with two fiber laser sources," in *Advanced Microscopy Techniques IV; and Neurophotonics II*, SPIE Proceedings (Optical Society of America, 2015), 953604.

1. Introduction

FDML lasers are narrow band, high-speed optical frequency swept sources [1] that have proven their value in many different applications such as optical coherence tomography (OCT) [2–8], stimulated Raman spectroscopy [9], picosecond pulse generation [10], and sensing [11–18]. Their main application is still high speed OCT, where they have enabled recent developments such as ultra-widefield retinal MHz-OCT [19, 20], high definition live 3D-OCT [21] and "Heartbeat OCT" [22, 23], all applications where multi-MHz A-scan rates are mandatory. The most important parameters of OCT sources, besides sweep rate, central wavelength, spectral shape and bandwidth, are noise and achievable roll-off performance. Many effects influence the performance of FDML lasers [24–29] and there are numerous indications that chromatic dispersion in the laser cavity is one of the most important [27, 30–32]. Kraetschmer and Sanders showed first, that a typical FDML laser intensity trace can exhibit nearly a hundred percent intensity modulation when measured with sufficiently high detection bandwidth of ~ 4 GHz or more [33]. Depending on the FDML operation parameters, Slepneva et al. identified the observed fluctuations as Turing instabilities or fully chaotic behavior [27]. Interestingly, when the FDML laser output intensity is measured with moderate photo receiver bandwidth of up to ~1 GHz, the output appears very smooth, indicating that the instabilities contain mainly very high frequencies, but still they cause a degradation of OCT images, even if the system only measures up to several hundred MHz electronic bandwidth.

However, Kraetschmer and Sanders pointed out that an ultra-stable mode locked behavior centered around a very narrow range at the laser's zero dispersion wavelength exists when the cavity is very well dispersion compensated [33]. This range can be identified by the CW tuning steps described in [27]. In this very small (3.5 nm in their laser) spectral region that Sanders termed "sweet spot", the intensity variation within one sweep is vastly reduced. Up to at least several milliwatt, shot noise is dominant in the laser output, i.e., no excess noise can be measured. Sanders also reported instantaneous linewidths of ~100 MHz corresponding to meters of coherence length. Thus, this sweet spot operation would be extremely interesting for biomedical imaging, spectroscopy and sensing. Since this sweet spot was observed around

the zero-dispersion wavelength of the FDML laser, additional dispersion compensation might extend this range. However, it has not been investigated yet, which amount of dispersion compensation is needed for a more than 100 nm sweep range FDML laser with all sweet spot operation. So far, nobody demonstrated a sweet spot wider than ~6 nm. Here we demonstrate our implementation of an FDML laser operating in this ultra-low noise sweet spot mode throughout a 118 nm sweep range at a center wavelength of 1292 nm and demonstrate drastically improved OCT image quality.

2. Setup

Figure 1 shows the schematic of our improved FDML laser. The basic principle of our wavelength swept FDML laser is to drive a tunable optical bandpass filter in resonance with the optical roundtrip time of light in the laser cavity [1] and to use a chirped fiber Bragg grating (CFBG) to cancel chromatic dispersion of the laser cavity [31, 32]. The entire FDML laser fiber cavity is integrated into a 3U height, temperature controlled 19 inch rack enclosure. The main components, semiconductor optical amplifier (SOA), fiber Fabry-Pérot filter (FFP), CFBG and delay fiber spool, all have their own active temperature regulation and are in part (SOA, spool) thermally isolated from each other. The high stability 8-channel Peltier temperature controller unit, which we built in house, has a theoretical resolution of 0.001 °C and an estimated stability and reproducibility of 0.01 °C. The accuracy was not perfected since it is not relevant for this experiment; it is estimated to be ~ 0.1 °C if no calibration step is performed.
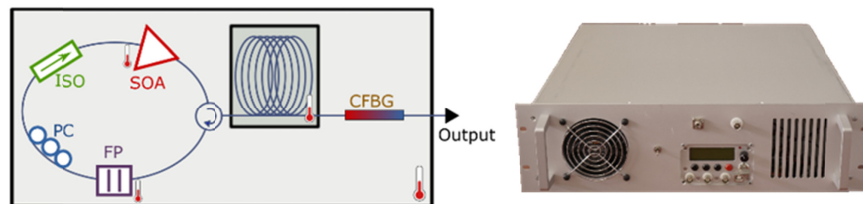

Fig. 1. Schematic and photo of the FDML laser: It comprises a 1310 nm semiconductor optical amplifier (SOA), a fiber polarization controller (PC), a fiber optic isolator (ISO), a fiber Fabry-Pérot filter (FFP) driven at 411kHz, a mixed fiber spool, and a custom made chirped Fiber Bragg Grating (CFBG).

The whole cavity is an 8:1 mix of Corning HI1060 and SMF28e fiber. The use of HI1060 fiber in the delay spool shifts the zero dispersion wavelength of the cavity out of the sweep range to enable simple dispersion compensation using a single custom made chirped fiber Bragg grating (CFBG made by Teraxion Inc.). To reduce overall cavity losses, the CFBG (~40% transmission) serves as an output coupler. The dispersion of this CFBG can be fine-tuned by applying a temperature gradient along the fiber; its retention plate is in contact with one Peltier element at each end. The homebuilt fiber Fabry-Pérot tunable filter (FFP) has its mechanical resonance at 411 kHz. The SOA is modulated to operate at 1/8 duty cycle to allow 8 times optical buffering, an optical time multiplexing technique of the sweeps [34] for a resulting wavelength sweep repetition rate of 3.28 MHz. For OCT imaging a buffer stage, booster [35], interferometer and detection unit described in an earlier publication [22] were used.

3. Measurements of FDML laser output at high detection bandwidth

To gain insight into the dynamics of FDML lasers in general, and the highly dispersion compensated and temperature stabilized FDML laser in particular, intensity traces were acquired with a 50 GHz photodiode (Finisar XPDV2320R) and a 63 GHz, 160 GS real time oscilloscope (Keysight DSOZ634A). The optical bandwidth of the FFP filter inside the laser cavity is $\Delta\lambda = 165$ pm corresponding to an optical frequency span of 29 GHz at 1300 nm

wavelength. Hence the > 50 GHz electronic detection system should be able to catch almost all intensity fluctuations of the laser (see chapter "theoretical considerations").

To achieve the desired low noise sweet spot operation at not only one or two narrow regions, but over the full sweep of the laser, the intracavity dispersion was mostly cancelled by a CFBG whose dispersion was then optimized manually by tuning its temperature gradient until the sweet spot covered the full sweep range. The sweet spot could easily be identified as a low noise section in the transient intensity traces acquired with the 50 GHz RF bandwidth. The remaining group delay (GD) differences in the cavity throughout the sweep range were difficult to measure but we estimate them to be below 200 fs throughout the full sweep range. This estimation is based on the accuracy within which the filter drive frequency had to be set.

As in Fig. 2, showing one forward and one backward 118 nm sweep within one drive cycle of the filter, most of the time the photodetector noise is dominant. However, sometimes high frequency modulations of the intensity build up that persist many cavity roundtrips. To get an impression of the dynamics throughout consecutive sweeps we created a movie animation (Visualization 1). Though these intensity modulations often group at the same spectral region, they can appear as completely isolated events, where the intensity suddenly falls, followed by an overshoot, probably due to the population inversion build up (gain recovery) during the laser off time. In the following we will call such events holes.
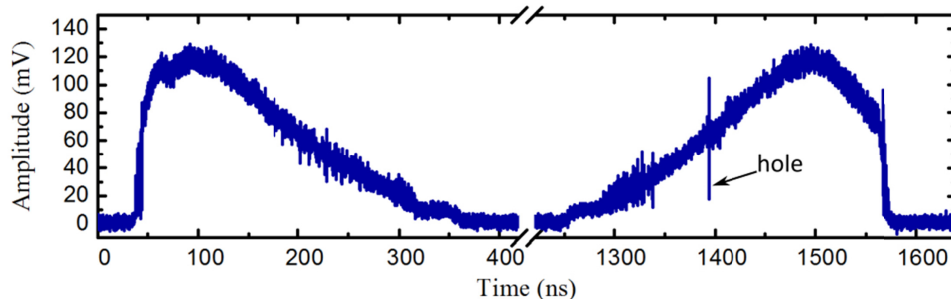

Fig. 2. Photoreceiver signal of intensity trace with 117nm sweep bandwidth of the FDML in ultra-low noise sweet spot mode. Shown are two consecutive sweeps, one backward (red to blue) and one forward sweep. The trace was acquired with 50 GHz analog bandwidth and 160 GS/s (for a video showing dynamic changes in consecutive sweeps see Visualization 1).

The "sweet spot" operation could not be extended to longer wavelengths, presumably due to remaining higher order dispersion or maybe also due to water vapor absorption lines present in the free space FFP. The absorption bands are visible in the ASE intensity spectrum which is shown together with the output spectrum of the laser in Fig. 3(a). Here they are caused by water molecules in the air within the optical spectrum analyzer (OSA). For future implementations and higher frequencies we will use a shorter wavelength shifted SOA to avoid these water vapor lines, which also impair overall OCT image quality [36]. The 3 dB width of 77 nm and the 10 dB width of 117 nm can be read from Fig. 3(b) showing the output spectrum on a linear scale.
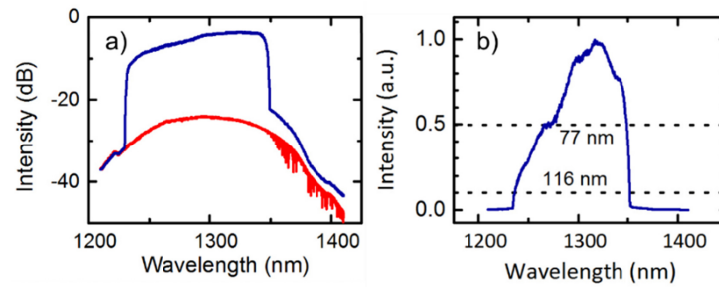
Fig. 3. a) Spectra acquired with an optical spectrum analyzer (OSA). Blue line: 117 nm full range FDML laser spectrum, centered at 1292 nm. Red line: Spectrum of ASE, showing the absorption lines of water vapor. b) The laser output spectrum on a linear scale showing the FWHM of 77 nm and the 10 dB width of 116 nm.

The sweet spot filter drive frequency band over which the laser can run without, or with very few intensity modulations, covers only a few millihertz. Detuning the frequency by one mHz at a nominal frequency of 411 kHz equals to 2.4 parts per billion (ppb). Once the inverse frequency of the FDML laser matches the cavity round trip time (RTT), there are two main causes of slow drift in open loop operation. The first one is a frequency drift of the main electronic clock oscillator in the function generator that drives the FFP. Thus, we used an oven-controlled crystal oscillator (ABRACON AOCJY3-10MHz) with a frequency stability of 5 ppb. Experiments with a rubidium atomic clock (unknown model) were not satisfactory, because although the atomic clock exhibited extremely high long-term stability, the short-term phase noise appeared to be a problem. The second issue is that a temperature drift within either the CFBG or the cavity of 0.01 °C will change the refractive index of the fiber by roughly 100 ppb equivalent to 29 mHz.
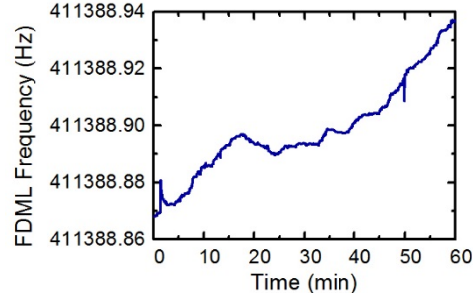

Fig. 4. Typical drift of the sweet spot frequency due to temperature changes in the FDML laser cavity.

Figure 4 shows the drift of the frequency over time. Within 1 hour, we see a drift of less than 100 mHz. This corresponds to a temperature variation of 0.17 °C, which exceeds the 0.01 °C stability of our Peltier controllers. Most likely, this is due to imperfections in the thermal engineering of the temperature spreaders in the laser cavity leading to deviations of the effective temperature from the temperature at the Peltier-element's sensor. Fortunately, the drift is very slow. This enabled us to keep the FFP frequency close to the sweet spot frequency using an automated regulation that keeps the laser within ± 1 mHz close to the optimum frequency. This regulation now enabled us to investigate the laser and its detuning behavior since we could repeatably set the resonant case as 0Hz and from there set a defined value of detuning. In the following sections, this strategy is used to systematically investigate the laser by measuring its noise.

3.1 Characterization of noise 1: intensity traces and noise spectra

While the cavity dispersion causes a wavelength *dependent* mismatch between the cavity RTT and the inverse FFP frequency, a detuning of the FFP frequency results in a wavelength *independent* mismatch between the two. As this mismatch seems to be the dominant effect causing intensity noise in FDML lasers, the effect of different amounts of remaining cavity dispersion can be simulated using different amounts of detuning. In Fig. 5 the intensity noise is shown in the time and frequency domain. The blue, black and red curves correspond to the different FDML frequency detunings from the optimum which are 0 Hz to 1 Hz and to 5 Hz respectively.
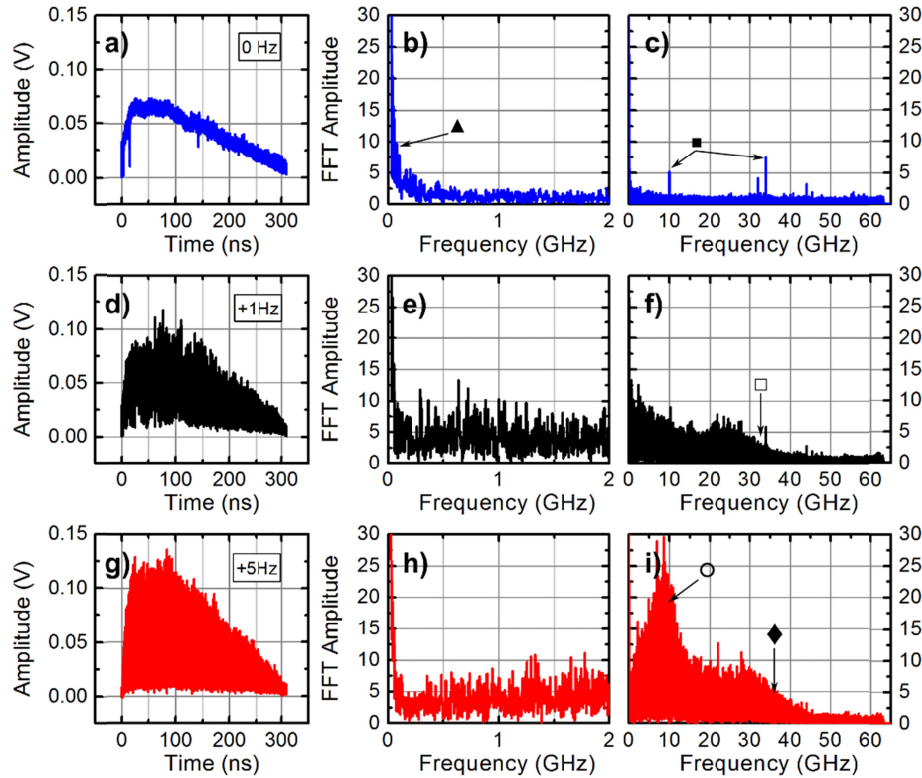

Fig. 5. Comparison of FDML laser intensity noise for 0 Hz (a,b,c - blue), 1 Hz (d,e,f - black) and 5 Hz (g,e,h - red) detuned FFP frequency. The output of the laser was recorded at 50GHz analog bandwidth. (a,d,g): Intensity traces, (b,e,h): Low frequency noise spectra plotted as amplitude of the Fourier transforms of the respective traces from 0 to 2 GHz on a linear scale.(c,f,i). Noise spectra over the full 63 GHz of the oscilloscope also on a linear scale.

The following described observations now have a dramatic impact on the most modern Megahertz OCT engines, since they commonly use 4 GSamples/s analog to digital converters, corresponding to up to 2 GHz analog detection bandwidth. Obviously, the lowest noise case is the resonant one (0 Hz) but this can actually not always be realized. Previous FDML lasers had so much remaining cavity dispersion that is was not possible to achieve the "0 Hz" resonant condition throughout the entire sweep. The intensity noise in the slightly detuned parts of the sweep generates noise in the OCT image which can be reduced by intentionally detuning the FDML laser by at least several Hertz – depending on the remaining cavity dispersion. This effect and its consequences for OCT image quality will be further analyzed in the following chapters.

When detuning the FFP frequency by 0 Hz, i.e. when the filter frequency is optimized using the frequency control loop (blue curves), the intensity time trace (Fig. 5(a)) exhibits

very low noise (considering the high electronic bandwidth). The noise spectrum (Fig. 5(b) and c) is flat and at a very low level over most of its range such that even the interleaving spurs caused by the oscilloscope electronics are now visible as spikes in the amplitude spectrum (Fig. 5(c), label ■). The increase towards low frequencies (Fig. 5(b), label ▲) is mainly caused by the intensity envelope itself.

Detuning the FFP frequency by 1 Hz (Fig. 5(d),e,f - black curves) raises the intensity noise in the time traces to modulation depths up to 100% (Fig. 5. d). Accordingly, the corresponding noise floor in the spectrum is also increased, but interestingly only up to ~30–40 GHz (Fig. 5(e) and f). This decrease between 30 and 40 GHz (Fig. 5(f), □) is not caused by the electronic bandwidth of the detection, which is 50 GHz. The noise suppression is most likely caused by the FFP filter in the FDML laser, which effectively causes low pass filtering of any amplitude and phase fluctuations of the laser light. The FFP filter has an optical bandwidth of 0.165 nm which corresponds at a wavelength of 1300 nm to an optical frequency bandwidth of 29 GHz.

Detuning of 5 Hz causes an almost full 100% intensity fluctuation (Fig. 5g) over the full sweep duration and the level of the noise spectrum is substantially raised (Fig. 5(i)). Additionally, a noise peak around 8 GHz can be observed which may be caused by relaxation oscillations linked to the carrier dynamics in the semiconductor gain medium of the FDML laser (Fig. 5(i), ○). The noise decrease between 30 and 40 GHz can be observed again (Fig. 5(i), ♦). Most interestingly the intensity noise towards low frequencies is actually lower than in the case of 1 Hz detuning (Fig. 5(e) and 5(h)). To better visualize this effect, the average of 1000 FFTs over a range of 0 to 6 GHz is shown in Fig. 6. Between 0 and 2 GHz the 5 Hz detuned FDML laser has lower noise than the laser at 1 Hz detuning, for higher frequencies the noise of the 5 Hz detuned laser is higher. However, both detuned cases have much higher noise than the 0 Hz case.
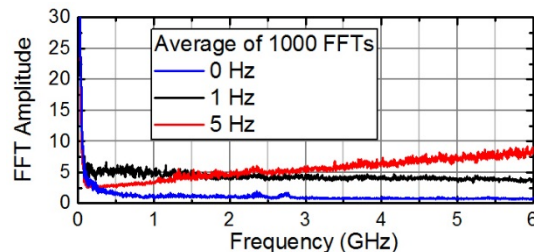

Fig. 6. Comparison of the noise spectra between 0 Hz and 6 GHz for 0 Hz (blue), 1 Hz (black) and 5 Hz (red) detuning. For each plot 1000 time traces were recorded and Fourier transformed. The FFTs were averaged and the amplitude values are plotted on a linear scale.

3.2 Characterization of noise 2: counting holes

In the previous section we investigated the situation for a detuning of several Hz where we observe noise in form of intensity fluctuations throughout the whole sweep. For smaller values of detuning ($\lessapprox$ 100 mHz) most of the intensity trace is "noise free" and we just observe some remaining isolated holes in the sweep as shown in Fig. 2 and Visualization 1. Since most of these holes have a duration of only 50 picoseconds or less they do not contribute substantially to the integrated noise over the 300 ns sweep and thus cannot be identified as increased noise in the noise spectrum. In order to still be able to characterize such low values of intensity noise, we switched to a different technique: we investigate the intensity trace and count the number of such holes as a measure for the remaining noise.

To quantify how the occurrence of holes qualitatively scales with the detuning of the FDML frequency, an algorithm applied a threshold below the mean intensity level and counted these intensity modulations that crossed this threshold as holes. Figure 7(a) shows the number of holes plotted against the detuning from the global sweet spot frequency over a

range of ± 2 Hz. There is a clear asymmetry with respect to the 0 Hz sweet spot frequency in both, forward and backward sweep. A similar asymmetry has been observed in experiments and simulations for many parameters of detuned FDML lasers [10, 24, 27, 34].

If we investigate the number of holes over a narrower range of detuning values of only ± 50 mHz (Fig. 7(b)), we still see a stable and comparably smooth curve with low noise. It can clearly be seen that even down to a range of a few millihertz stable characteristics can be identified with a distinct minimum.

Such a counting based method is employed in our frequency regulation circuitry which makes it very reliable, robust against external noise interference and long-term stable [37]. The stability of the frequency regulation of around 1 millihertz is good enough to operate the laser in a mode with very few holes per sweep. Thus, as will be shown in the following chapters, a good OCT image quality can be achieved even with active frequency regulation.
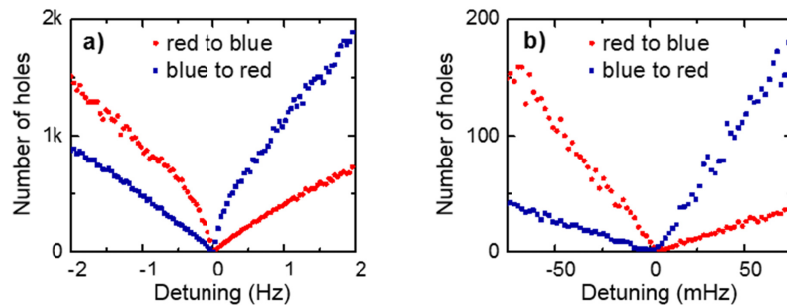

Fig. 7. (a) Number of holes per sweep at varying detuning from the sweet spot frequency. (b) Number of holes at different frequencies in the region very close around the sweet spot frequency.

3.3 Fringe contrast roll-off and high frequency fringes

The reduced intensity noise of the laser comes hand in hand with a vastly reduced phase noise. To demonstrate this, we measured the fringe contrast at different delays in arm lengths of a Michelson interferometer with the high speed oscilloscope. As can be seen in Fig. 8(a), the fringe contrast decreases by less than 40% at 8 cm reference arm delay. It should be noted that this fringe contrast does not directly translate to an OCT signal roll off, because it can be difficult to properly linearize the OCT signal in k-space at high frequencies with the required precision. However, we were able to demonstrate that this laser enables live 3D-OCT with imaging ranges of up to 10 cm in preliminary results [38]. The decrease in intensity noise goes hand in hand with a reduction in phase noise as seen in Fig. 8(b). It shows a typical section of a ~28 GHz fringe at 0 Hz detuning near the center of the sweep at ~1300 nm (Fig. 8(b) – bottom) and for 100 mHz detuning (Fig. 8(b) – top). It can be seen, that in the 0 Hz resonant case we observe a very regular fringe signal indicating good phase stability. In general, we observe such a regular signal in all regions of the sweep without holes. For the detuned case by 100 millihertz numerous phase and amplitude fluctuations are obvious. So this means that the low noise FDML laser does not only exhibit improved intensity noise but also has better coherence properties.
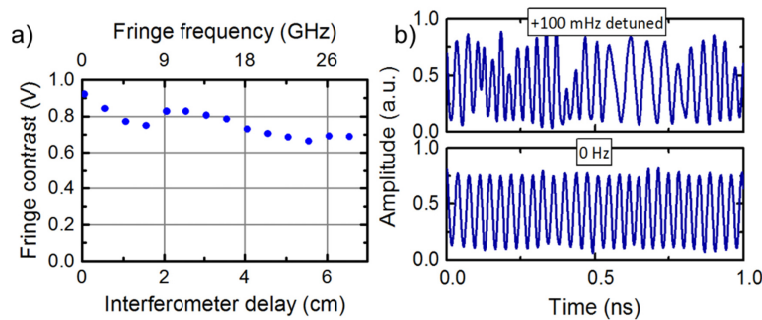
Fig. 8. (a) Fringe contrast roll-off with automated frequency regulation keeping the laser in the low noise operation mode. (b) Comparison of ~28 GHz fringes in low noise operation and with a detuning of + 100 mHz.

3.4 Comparison to our prior FDML laser implementations

Figure 9 compares our new laser with two additional FDML lasers having different, larger amounts of cavity dispersion. In Fig. 9(e) the respective dispersion of all three lasers is plotted as the round-trip time mismatch.

Figure 9(a) shows the output of an FDML laser whose cavity is all SMF28 fiber only. Operating at comparable parameters (363 kHz drive frequency of the FFP, 1/8 duty cycle allowing eight-fold optical buffering), it shows a dramatically higher intensity noise. Again, the dominant noise contribution stems from holes where the intensity drops from the mean intensity level to often almost zero, followed by a spike. In this laser, the mismatch between RTT and inverse FFP frequency varies within approximately 80 picoseconds when the FFP is adjusted so that both sweet spots fall within the sweeping range as can be read from Fig. 9(e). The sweet spots, where the RTT exactly matches the filter driving frequency can easily be found as permanent low noise areas within the sweep.

As another example two sweeps of an FDML laser using a CFBG to reduce the cavity dispersion are shown in Fig. 9(b) and (c). In this laser (also 363 kHz, 1/8 duty cycle), the remaining RTT mismatch varies within a few picoseconds only (see Fig. 9(e)) and the noise is visibly reduced. However, the noise distribution and markedness within the sweep varies strongly from sweep to sweep which we attribute to the not perfect temperature stability of the cavity. In contrast, the distribution of the holes in the new laser, when it is detuned from the optimum frequency by 100 mHz corresponding to a constant RTT mismatch of 0.6 ps, is very uniform as can be seen in Fig. 9(d).

These measurements show that the timing error caused by remaining cavity dispersion in some parts of the sweep and frequency tuning of the filter can have a similarly negative effect on the noise performance. Hence, for a good FDML laser, it is necessary to compensate dispersion very accurately and at the same time ensure an extremely accurately synchronized driving frequency of the filter.

Considering that increased detuning can reduce intensity noise at low frequencies, this implies that a moderately dispersion compensated laser does not necessarily offer decreased intensity noise compared to a poorly dispersion compensated one.
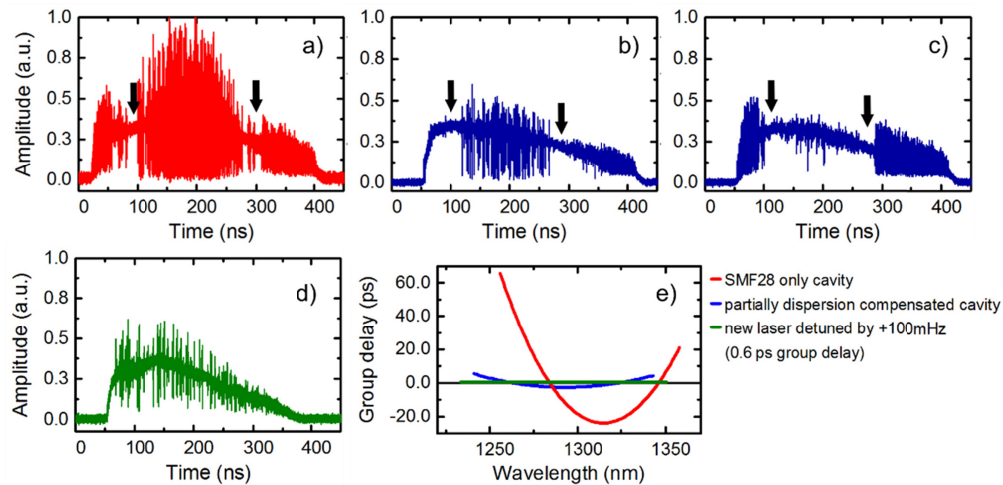
Fig. 9. FDML laser intensity outputs acquired at 50 GHz detection bandwidth. (a) Laser with an all SMF28 fiber cavity without a CFBG for dispersion compensation sweeping over a 104 nm spectral range at a center wavelength of 1307 nm. The black arrows indicate two "sweet spots". (b,c) Two sweeps from an FDML laser with imperfect dispersion compensation sweeping 110 nm at 1292 nm. (d) The new laser detuned from the optimum frequency by 100 mHz. (e) Calculated mismatch of cavity round trip time and inverse FFP frequency.

4. Discussion

Numerical simulations by Slepneva et al. suggest, that the holes observed in our experiment, i.e. the intensity instabilities which can be observed with high speed electronic detection [27, 33], can most likely be identified as Nozaki-Bekki holes [39]. These Nozaki-Bekki holes are a localized amplitude depression found in solutions of the Ginzburg-Landau equation [40, 41]. However, a theoretical description of these holes is not the focus of the paper.

To reach an intuitive physical understanding of the dynamics and more so about the reason for why the holes initially exhibit very deep (almost 100 % - see Fig. 9) intensity modulation, we suggest the following simple model: We consider the light roundtrip through the FDML laser cavity starting from the exit facet of the FFP, propagating through the cavity and ending at the input facet (Fig. 10(a)). In a recent publication we showed that in the ideal case, the light field inside the FFP is Doppler shifted in a way such that it always matches the new wavelength of the light arriving, which traveled the "long" way through the cavity to the input facet [25]. However, obviously it is required that the light field arrives at the input facet of the Fabry-Pérot with the correct phase.

When the light incident on the FFP is significantly out of phase to the field stored in the cavity for many optical cycles, most of it is reflected and the light field inside the FFP can deplete within its storage time for the electric field. This requires a fast phase shift (in addition to the smooth, continuous phase shift created by the k-sweeping of the filter) within a sweep. These phase shifts might be caused by dispersion in the cavity and the CFBG or intensity dependent effects in the SOA. An indication for the relevance of remaining temperature instabilities is the fact that the laser exhibits a slightly higher number of holes during the first minutes of the warm up phase.

In the sweet spot operation mode, this model suggests that intra-sweep phase variations are small enough, so that the electric field inside the FFP cavity can adapt its phase to the optical phase of the light coming back from the feedback delay without ever being depleted. Even though the light field stored inside the FFP can adapt to phase variations in the feedback we think that a passive dispersion compensation mechanism is necessary to enable the all sweet spot operation. This assumption is based on the fact that a RTT mismatch of a certain wavelength – even if less than an optical period (4.3 fs at 1300 nm) – circulating the cavity

causes a cumulative temporal offset to the FFP phase requiring that the light is reflected after some roundtrips. We suggest two possible linear effects that might help to *passively* compensate the chromatic dispersion: First, the polarization may vary slightly within an FDML laser sweep [26, 42]. Different polarization modes exhibit different optical path lengths due to bending strain induced birefringence in the fiber allowing any wavelength to "choose by itself" its optimum polarization within the restrictions of polarization dependent components such as the SOA. The second effect is related to the group delay of the FFP, which we think is the dominant contribution. In short, the FFP sweep filter generates different amounts of group delay, depending on how far the transmitted light wavelength is offset from the peak transmission. Slightly asynchronous operation can then generate a self-stabilizing situation. This effect will be explained and characterized in more detail in the next section.
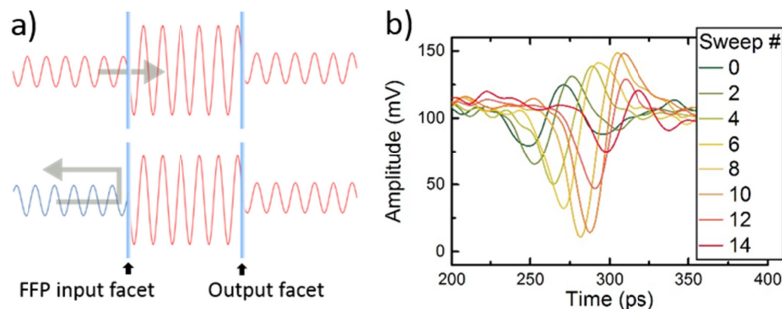

Fig. 10. (a) Simple model for the phase disturbances causing the holes. When the incoming light field to the FFP changes its phase so fast that the light in the FFP cavity cannot accommodate adiabatically, the feedback light is reflected, and the light stored in the FFP depletes. (b) Intensity traces that show the evolution of a holes within 15 consecutive sweeps. All traces were acquired at the same temporal position relative to the FFP filter drive signal.

There are many interesting effects such as the movement of the holes in intensity traces from sweep to sweep (see Fig. 10(b)), grouping of holes, reoccurrence at the same spectral position of holes, increased phase noise in fringes when holes are present and more, but these observations would require further studies and are outside the scope of this paper. Several of these effects have been described in a quasi FDML operation by Slepneva et al. in the paper "Turbulent laser puffs" [43]. The spike though, following the vast majority of these holes is quite likely to be an overshoot, as the population inversion in the SOA recovers during the laser's off-time - so this is simply a carrier relaxation / gain recovery oscillation. It seems like these holes are the dominating source of noise in this FDML laser and while the following theoretical considerations and analytical model of these holes are not meant to fully describe the behavior of our extremely well dispersion compensated laser, we think they can give a more intuitive understanding of the behavior than fully numerical simulations of FDML laser noise only. It should be noted that we can also observe more chaotic noise behavior, dominantly occurring on one side of the detuning curve, depending on the sweep direction, for larger values of detuning. In contrast, the noise which we observe in the long wavelength region, appears to have some quasi-periodic structure which might resemble the Turing instabilities suggested in [27]. We cannot surely identify the reason for this noise, because on the one hand, it lies exactly in the region of the water vapor absorption line, on the other hand this is a region where we have a higher remaining cavity dispersion.

5. Theoretical considerations

5.1 Phase jumps

We suggest that the holes we see in the output intensity of the FDML laser occur when the field of light reaching the input facet of the Fabry-Pérot filter has a significantly different

phase than the light stored inside the Fabry-Pérot filter. As mentioned above, such phase shifts can for example be introduced by effects such as fiber dispersion, birefringence and nonlinearity, a drift of the sweep repetition rate or optical path length changes due to temperature fluctuations. This phase shift accumulated during a round trip can be modelled by a phase jump of the incoming optical field, influencing the transmitted and reflected intensity of the Fabry-Pérot cavity which can be treated analytically. As shown in [25], the FFP action on the synchronously wavelength-swept optical field can be described by its stationary transmission characteristics. Consequently, for a phase jump by an angle Δ_φ at $t = 0$, an exponentially decaying response is obtained, i.e., the transmitted intensity (normalized to the incoming one) is

$$\tilde{I}_t(t) = 1 + 2\sigma(t)\left[\cos\left(\Delta_\varphi\right) - 1\right]\left[e^{-\pi\delta_f t} - e^{-2\pi\delta_f t}\right],$$

and the reflected intensity is

$$\tilde{I}_r(t) = 2\sigma(t)\left(e^{-2\pi\delta_f t}\right)\left[1 - \cos\left(\Delta_\varphi\right)\right].$$

Here $\sigma(t)$ is the unit step function, and $\delta_f = \lambda_0^{-2} c \delta_\lambda$ where δ_f and δ_λ are the FWHM of the sweep filter with respect to frequency and wavelength, respectively, and λ_0 is the central wavelength. Figure 11 shows the result for $\Delta_\varphi = \pi$.
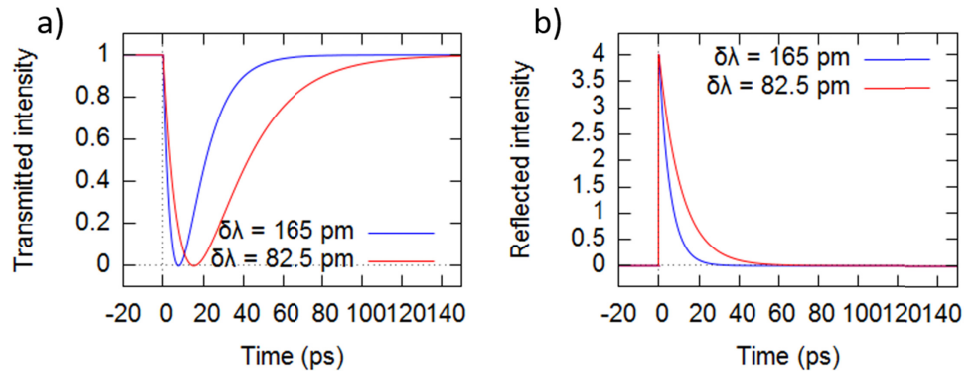

Fig. 11. Calculated transmitted and reflected intensities before and after a phase jump $\Delta_\varphi = \pi$ at $t = 0$ for 165 pm and 82.5 pm FWHM FFPs.

The simulation nicely reproduces the experimentally observed holes and their timescales, see Fig. 11(a). Furthermore, above model intuitively explains the experimentally observed suppression of intensity noise below the measurement limit in the low dispersion regime: For small phase shifts Δ_φ, we obtain $\cos(\Delta_\varphi)-1 \approx -(\Delta_\varphi)^2$ and thus quadratically reduced intensity modulations, which are further suppressed by above mentioned passive stabilizing mechanisms, in particular the FFP group delay mechanism discussed in detail below.

The filter bandwidth imposes a lower limit for the rise and fall times in the transmitted field, so we don't expect hidden intensity fluctuations at frequencies we cannot detect with our 50 GHz detection bandwidth. As the temporal extent of the holes scales inversely proportional with the filter bandwidth, employing an FFP with smaller filter window will increase the rise and fall times of the holes and make them visible at lower detection bandwidths. This might increase the noise in OCT applications, where the comparatively low detection bandwidth filters the high frequency amplitude modulation imposed by the holes. This assumption is consistent with earlier observations by Biedermann et al. [30]. However,

the also increased group delay of such a filter might further reduce the occurrence of such holes by passive phase stabilization as will be explained in the next paragraph.

5.2 FFP group delay and dispersion compensation

As mentioned, we credit a major role for the compensation of the dispersion in the laser cavity to the Fabry-Pérot filter. Like any bandpass filter, the FFP induces a group delay on the incoming signal. The amount of group delay depends on the frequency offset relative to the maximum transmission frequency. In the following, we will show how this frequency dependent group delay could act as a passive dispersion compensation mechanism.

The dispersion relation of the FFP is that of an ordinary bandpass filter and can be treated analytically. Using the convention $e^{-i\omega t}$ for a plane wave and frequency offset f, the group delay is defined as $\tau_g = \dfrac{d\varphi}{d\omega}$. Thus, with the sweep filter amplitude transmission given by

$$t_s = \frac{T_{max}^{1/2}}{1 - 2if/\delta_f} = \frac{T_{max}^{1/2}}{1 + 4(f/\delta_f)^2}\left(1 + 2if/\delta_f\right),$$

we obtain

$$\varphi = \tan^{-1}\left(2\frac{f}{\delta_f}\right)$$

and

$$\tau_g = \frac{d\varphi}{d\omega} = \frac{1}{\pi\delta_f}\frac{1}{1 + \left(2f/\delta_f\right)^2}.$$
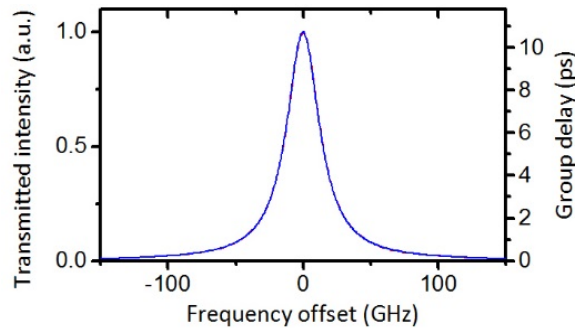

Fig. 12. FFP intensity transmission normalized to the maximal transmission and group delay dependence on the light's frequency offset relative to the filter transmission window center.

Figure 12 shows the group delay for light that arrives at the FFP with a frequency difference relative to the transmission window for a filter with a spectral width of $\delta_\lambda = 0.165$ nm centered at $\lambda_0 = 1292$ nm. Light with a frequency that exactly matches the maximum transmission of the filter experiences a group delay of 10 ps when passing the filter. Light with an offset relative to the transmission maximum experiences less group delay. For example, for a frequency offset of ± 15 GHz, the group delay induced by the filter reduces to only about 5 ps.

For a filter window moving in time, this suggests that any wavelength circulating the laser cavity may experience a varying GD in the FFP due to very small delays in the cavity. If the FFP filter frequency f_{FFP} is chosen such that

$$\max\left(RTT_{cavity}(\lambda)\right) < 1/f_{FFP} < \min\left(RTT_{cavity}(\lambda)\right) + GD_{FFP}^{max},$$

with $\min\left(RTT_{cavity}(\lambda)\right)$ and $\max\left(RTT_{cavity}(\lambda)\right)$ being the shortest and the longest roundtrip time for any wavelength through the cavity excluding the FFP, and GD_{FFP}^{max} being the maximum of the FFP filter group delay shown in Fig. 12, any active wavelength can pick a position in the filter window such that the total RTT exactly matches $1/f_{FFP}$. Of course, these temporal offsets must be sufficiently low so the FFP loss (reflected intensity) remains irrelevant. As the light will arrive at the FFP with a constant frequency offset after every roundtrip, as long as $RTT_{cavity}(\lambda)$ doesn't change, we will call this position stationary.

As shown in Fig. 13a, there are two positions for every wavelength in the filter window at which any given wavelength will exactly meet the FDML condition

$$1/f_{FFP} = RTT(\lambda) = RTT_{cavity}(\lambda) + GD(\lambda),$$

but as will be explained in the following, only one of them is stable.

When the inverse filter frequency of the FFP exactly matches the round trip time of the light (including the group delay given by the filter) for every wavelength in the sweep, the FDML laser can be run in a stationary mode with phase matching at the input facet of the FFP, again, as long as there are no changes in $RTT_{cavity}(\lambda)$. However, these changes will naturally occur continuously, for example due to temperature drifts in the cavity.

We now look at one arbitrary wavelength within this sweep that runs stationary in the negative wing (left half in Fig. 13a) of the filter transmission band. We assume that its RTT_{cavity} increases by a time τ due to a temperature drift in the cavity as sketched in Fig. 13b. When the light arrives delayed at the filter, the center transmission frequency has increased and the light hits the filter with an increased negative frequency offset (for the red to blue sweep). For example, a filter tuning over 100 nm at an A-scan rate of 3.2 MHz will have shifted its center transmission wavelength by ~ 1.1 GHz within 20 ps. Due to the increased negative filter offset, the light passes the FFP faster. This way the FFP group delay can compensate for a part of the delay τ in the cavity. In consecutive sweeps the wavelength under inspection will continue to experience the delay τ in the cavity and will wander to the left of the filter transmission window until the reduction in group delay of the filter equals τ. From then on it will run in a stationary mode as the RTT equals the filter drive period again. This is sketched in Fig. 13b with the red dots being positions in consecutive sweeps following the black arrow.

When the RTT_{cavity} of this specific wavelength decreases by $-\tau$, the group delay of the filter will increase and, again, after some roundtrips compensate for $-\tau$. This way, we think that the filter can compensate remaining dispersion in the cavity as well as wavelength dependent dynamic changes in the cavity length and therefore allows a stable operation with no or very few holes.

However, when the specific wavelength hits the filter transmission band with a positive frequency offset, any change of the frequency accelerates the wandering of this wavelength to the other border of the transmission window i.e. to the stable regime. The same argument works for the forward sweep, however, then the stable and unstable regimes depicted in Fig. 13 are interchanged.
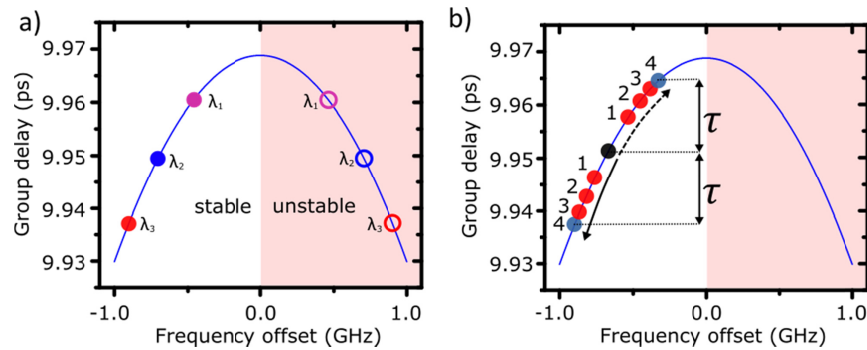
Fig. 13. FFP group delay dependence on the light frequency offset to the filter center frequency. a) Stable and unstable operating points with equal GDs. Any wavelength (colored circles) can experience a suitable group delay compensating for varying round trip times through the cavity by hitting the filter with either a negative or positive frequency offset. b) Stable operating point for a wavelength before (black dot) and after (blue dots) a change of its cavity round trip time $RTT_{cavity}(\lambda)$. The numbered red dots indicate the position in the filter window of the observed wavelength after consecutive round trips. The direction of the walk off caused by a delay in the cavity is indicated by the black solid arrow and the walk off caused by a decreased RTT is indicated by the black dashed arrow.

6. Imaging with a highly dispersion compensated FDML laser
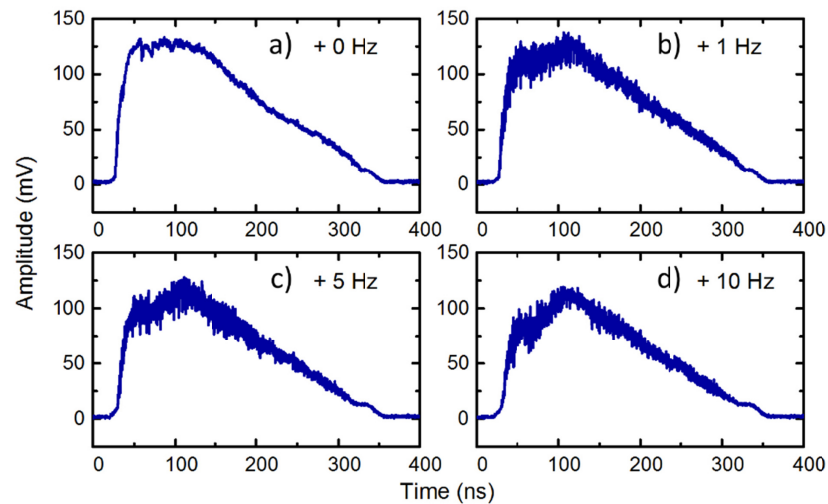
6.1 High frequency noise

Fig. 14. Intensity traces of a 110 nm sweep acquired at the sweet spot frequency (a) and with different detuning (b-d) of the FFP frequency. All traces have been numerically low pass filtered to 1.6 GHz.

It is surprising that such noisy FDML laser sweeps as seen in Fig. 9 can be used for shot noise limited detection of interference signals. However, this can be explained by the fact that the limited detector bandwidth in current OCT systems acts as a filter for the high frequency noise. Concerning MHz–OCT systems with their modern high-speed digitizers this causes a counterintuitive effect on the image quality. When the cavity dispersion of an FDML laser is reduced, perceived image quality may become worse as the laser appears to have more low frequency (< 2 GHz) noise. This can be nicely simulated by detuning our extremely dispersion compensated laser. Figure 14 shows intensity traces at different amounts of detuning, which are then numerically low pass filtered to 1.6 GHz cutoff.

At a 10 Hz detuning the laser noise seems to be reduced compared to a 5 Hz detuning. The reason for that seems to be that the holes occur very regularly, dense and uniformly distributed at very high detuning. Therefore, the average intensity per digitizer sample seems to be more stable. If the number of holes gets very high, the average measured power at limited electronic bandwidth statistically approaches the real value closer – simplified: as the number of events n rises, the relative fluctuation decreases proportional to $\sqrt{n}/n$. So, detuning a good but not perfectly dispersion compensated laser may therefore improve image quality with respect to noise, but of course, this comes at the cost of reduced coherence length and worse roll-off performance. This observation is consistent with the measurements plotted in Fig. 6.

6.2 Dynamic range limitation

In highly scattering media the penetration depth of OCT with MHz FDML lasers is clearly dynamic range limited. The presence of strong signals will raise the noise floor in an A-scan which drowns out small signals and therefore reduces the imaging depth. This effect is visible in OCT images as vertical stripes and scales with the distance of the highly scattering layer from the zero-delay position. Figure 15 shows 3 OCT images of a human finger knuckle joint acquired with the new laser at different detuning states of 0 Hz (Fig. 15(a)), 1 Hz (Fig. 15(b)) and 10 Hz (Fig. 15(c)). All images were acquired using a 1.6 GHz balanced photodiode (Thorlabs, PDB480C-AC) and a 1.5 GHz analog detection bandwidth, 4 GS/s, 8 bit digitizer (GaGe, CobraMax). As can be seen in the zoomed in sections, the noise level is the lowest at 0 Hz detuning. However, the noise seems to be slightly reduced in the case of 10 Hz detuning compared to the 1 Hz detuning. This agrees well with our finding that the intensity noise of the laser in this frequency range is the worst at a moderate detuning and also with the measurements plotted in Fig. 6.
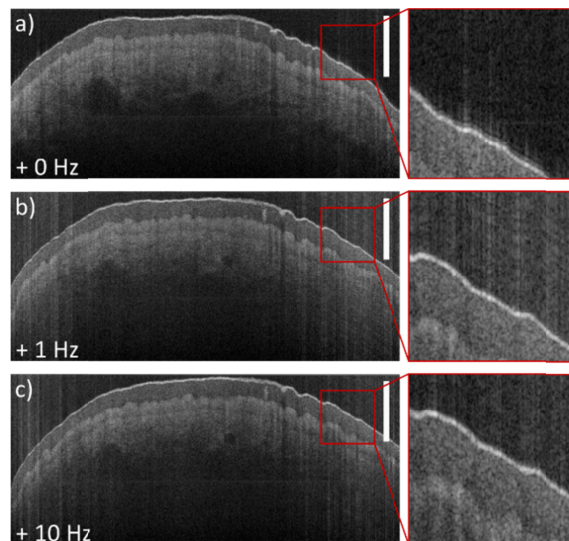

Fig. 15. 3.2 MHz A-scan rate OCT images (2048 A-scans at 40 mW light exposure) of a human finger knuckle joint acquired at different detuning from the sweet spot frequency. The white bar corresponds to 1 mm in tissue.

While balanced detection allows to eliminate the relative intensity noise (RIN) of the laser for shot noise limited signal detection even with poorly compensated lasers, balanced detection does not improve dynamic range, since this type of noise, generated by a high reflection, causes out of phase signals in the differential photodiode and cannot be balanced out. As it is visible in the images the increased temporal coherence of our highly compensated

FDML laser offers greatly reduced noise combined with improved roll-off performance. This improves the system's detectable dynamic range. In prior demonstrations of our live rendered 3D-OCT, aggressive cut levels had to be set to reduce the visibility of the vertical stripes at the cost of visibility of deeper lying structures. Still the vertical stripes were visible as artifacts. A direct comparison of live rendered 3D-OCT using the new laser and our prior work (see Fig. 16) shows a dramatic increase in image quality. The new extremely well dispersion compensated laser is therefore an ideal source for multi-MHz A-scan rate optical coherence tomography on difficult samples with bright reflections like intravascular imaging over metal stent structures, endoscopic OCT with remaining lens reflections, skin imaging without refractive index matching to air, anterior segment imaging of the eye etc.
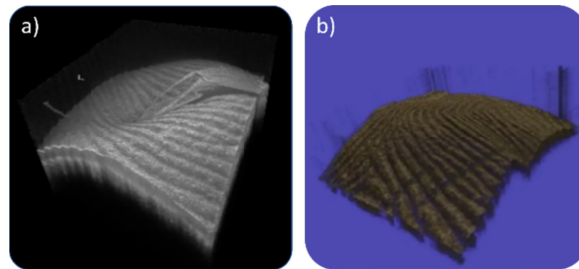

Fig. 16. Comparison of live rendered 3D-OCT using the new low noise FDML laser (a) to our prior work (b) (see Visualization 2).

7. Conclusion and outlook

The OCT images and video presented here clearly prove the huge impact of the presented work on the quality of images based on intensity contrast. In addition, imaging modalities making use of the complex phase to improve image quality [44–46] or to provide additional contrast [47–51] have gained increasing attention recently. Preliminary examinations show a great reduction of the sweep to sweep phase noise which will very likely benefit or ease the implementation of these techniques. Of course, any other technology besides OCT that requires rapidly frequency swept lasers [11, 52] could benefit from the low noise characteristics of the presented FDML laser as well. Finally, we observed indications for very good coherence roll off properties that will benefit future applications.

The experimental verification of theoretically predicted phenomena such as dark solitons and Nozaki-Bekki holes [39] are extremely interesting advances to the full understanding of the complex physics of the FDML laser and highlight its value as a great tool for theoretical laser physics. We think that the fine control of the cavity round trip time mismatches to the filter frequency will make the distinction and observation of these phenomena and the identification of different operating regimes [27] much easier.

From a physics viewpoint, the FDML sweep operation, free of any holes, is in so far highly interesting, as it should present a highly stable optical phase relation during the entire sweep. When the laser has an intensity hole and stops emitting, the light after such a hole most likely has an optical phase which is not correlated to the phase before the hole. This is, why current FDML lasers have a good correlation of the average phase over the whole sweep, but not necessarily a good local (meaning close spectral proximity) phase stability. In contrast, the "all sweet spot" FDML laser presented in this paper stores the phase in form of the adiabatically tuned light field inside the FFP [25]. Hence, a strong correlation of the local phase is promoted and it might be speculated if now FDML laser sweeps can be compressed to femtoseconds or if FDML laser frequency combs become feasible.

Funding

Disclosures

TP: Optores GmbH (P,R), MP: Optores GmbH (E), WD: Optores GmbH (I,P,R), RH: Optores GmbH (I,P,R), Optovue Inc. (P,R), Zeiss Meditec (P,R), Abott (P,R).